Results in Physics 56 (2024) 107247

Contents lists available at ScienceDirect

Results in Physics

journal homepage: www.elsevier.com/locate/rinp

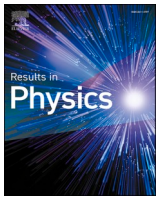

Determination of the energy loss function of tungsten from reflection electron energy loss spectroscopy spectra

Z. Li [a], J.M. Gong [a], Y. Harada [c], B. Da [c,*], R.G. Zeng [d], Z.J. Ding [a,b,*]

[a] Department of Physics, University of Science and Technology of China, Hefei 230026, Anhui, PR China
[b] Hefei National Laboratory for Physical Science at Microscale, University of Science and Technology of China, Hefei 230026, Anhui, PR China
[c] Center for Basic Research on Materials, National Institute for Materials Science, Tsukuba, Ibaraki 305-0044, Japan
[d] Institute of Materials, China Academy of Engineering Physics, P.O. Box 9071, Jiangyou, Sichuan 621907, PR China

ARTICLE INFO

Keywords:
Energy loss function
reverse Monte Carlo
Reflection electron energy loss spectroscopy
Sum rule
Tungsten

ABSTRACT

We incorporate experimental reflection electron energy loss spectroscopy (REELS) spectrum data with theoretical analysis to precisely determine the energy loss function (ELF) of tungsten (W) in the energy loss range of 0.1–110 eV at the incident electron energies of 1 keV, 2 keV and 3 keV. Employing the reverse Monte Carlo (RMC) method, we have obtained an averaged ELF whose relative errors of the perfect-screening sum rule and oscillator-strength sum rule were ~ 0.70 % and 0.68 %, respectively. This ELF was then used to derive the optical constants and complex dielectric function. Furthermore, we have successfully differentiated between bulk and surface contributions to the REELS spectra throughout the entire considered energy loss range.

Introduction

The refractory metal, tungsten, possesses the highest melting point and tensile strength among the pure metals, making it an ideal material for various applications, e.g. the filament of electron guns for scanning electron microscopy (SEM) [1] and tip for scanning tunneling microscopy (STM) [2]. Furthermore, tungsten compounds are important materials in optoelectronics [3–5] and energy-related applications [6,7]. In order to facilitate research and development of materials, Palik [8] has compiled an extensive database of frequency dependent optical constants, i.e. the refractive index $n(\omega)$ and extinction coefficient $k(\omega)$, at the long wavelength limit ($q \rightarrow 0$). Those data were measured by different optical methods and by various research groups, encompassing most metals and some compounds. For tungsten the Palik's database comprises two datasets: the measured data covering the energy loss range of 0.15–33 eV by Weaver et al. [9] and the calculated data using atomic scattering factor in the photon energy range of 100–2000 eV by Henke et al. [10]. The optical energy loss function (ELF), $\mathrm{Im}\{-1/\varepsilon(\omega)\}$, describing the electronic excitation characteristics has relationship with optical constants: the real part of the complex dielectric function $\varepsilon = \varepsilon_1 + i\varepsilon_2$ is $\varepsilon_1 = n^2 - k^2$ and the imaginary part is $\varepsilon_2 = 2nk$. However, the measured photon energy range of the ELF of tungsten in the Palik's database is not complete and there is no data in the range of 47–100 eV. Below hundred eV the electronic excitation of a solid is quite different from that of atoms; then the Henke's data for atoms lose accuracy for description of metal in the low photon energy region. The absence of data certainly limits its application.

On the one hand, the electron energy loss spectroscopy (EELS) [11,12] can provide an alternative way for deriving useful information about the dielectric response of a solid to an external electric field carried by electrons. However, the EELS technique utilizes an extremely high energy beam and a free-standing thin sample in a transmission electron microscope, both are rather strict limitation in experiment. Therefore, the reflection electron energy loss spectroscopy (REELS) technique with surface electron spectrometer in a low cost instrument has emerged. The most evident advantage of employing REELS is its capacity for a quick measurement in a wide range of electron energy loss (corresponding to photon energy in the optical methods), about one hundred eV, with a single spectrometer; this range is much broader than that of an optical method utilizing a specific light source. In addition, there is no need of high beam energy and special preparation of the sample. This helps also to minimize the potential systematic errors that may arise from conducting multiple experimental measurements using different instruments.

On the other hand, there is a challenge in the REELS data analysis as

* Corresponding authors at: Center for Basic Research on Materials, National Institute for Materials Science, Tsukuba, Ibaraki 305-0044, Japan (B. Da). Hefei National Laboratory for Physical Science at Microscale, University of Science and Technology of China, Hefei 230026, Anhui, PR China (Z.J. Ding).
E-mail addresses: DA.Bo@nims.go.jp (B. Da), zjding@ustc.edu.cn (Z.J. Ding).

https://doi.org/10.1016/j.rinp.2023.107247
Received 19 October 2023; Received in revised form 3 December 2023; Accepted 3 December 2023
Available online 7 December 2023

the REELS spectrum involves combined effects from surface excitation, multiple inelastic scattering and elastic scattering. The surface effect must be excluded since the ELF represents only the bulk property. Multiple scattering effect and also elastic scattering effect needs to be removed since ELF represents only the electron inelastic scattering property or electronic excitation characteristics of the solid. Many studies have already been undertaken to understand the physical mechanisms within experimental REELS spectra and, hence, to extract the bulk dielectric function or ELF. Ohno [13] simply considered a direct proportionality between the normalized intensity of a REELS spectrum and the ELF, without excluding the surface effect. Yubero and Tougaard [14] have developed a more realistic model for quantitative analysis of inelastic cross sections and have evaluated ELF by a trail-and-error procedure [15]. Ding et al. [16,17] have developed a Monte Carlo simulation model for electron interaction with a surface to simulate the REELS spectra, by considering a spatially varying differential inelastic scattering cross section model for electron inelastic scattering in the surface region [18–20]. A deconvolution procedure was proposed by Werner [21] to obtain the normalized differential inverse inelastic mean free path (DIIMFP) as well as the differential surface excitation probability through two REELS spectra under different experimental conditions; this technique has been put to use to extract ELF for some elemental metals [22]. Da et al. [23,24] have put forward a different approach, named as reverse Monte Carlo (RMC) method, for extracting the ELF from a measured REELS spectrum. This method, by merging Markov chain Monte Carlo (MCMC) sampling of oscillators in an analytical formulation of ELF [25] with a Monte Carlo simulation of electron interaction with a solid surface, accurately describes the electron scattering behavior in a REELS experiment and naturally removes all the effects from surface excitation, multiple inelastic scattering and elastic scattering [26].

In the primary RMC method [23,24] a straightforward linear combination of surface and bulk ELF components was harnessed to compute the DIIMFP. Later, further improvements have been made on the electron inelastic scattering modeling, encompassing the depth-dependent DIIMFP which is a complex combination of surface and bulk excitation terms in a semi-classical electron inelastic scattering model [27–29]. This improved RMC method has been quite successful in obtaining the optical constants for some solids, and the high accuracy of the derived data was confirmed from the sum rules [30–37].

In this work, we derive ELF of tungsten from the measured REELS spectra at the incident electron energies of 1 keV, 2 keV and 3 keV in the energy loss range of 0.1–110 eV by the RMC method. The accuracy of ELF is verified by sum rules [38]. Thereby, optical constants and dielectric function are also obtained, which are beneficial for the computation of electron inelastic mean free path, backscattering coefficient, secondary electron yield and other physical quantities in materials science.

Experiment

The experimental setup for the REELS measurements was similar to the previous one employed for the SiO_2 measurements [24], except that the experiments for tungsten were carried out without the inclined sample holder. Before the REELS measurements, the tungsten sample was sputtered by Ar^+ for cleaning and removing the surface contamination, and the cleanness was checked by Auger electron spectroscopy. The REELS spectra of the cleaned tungsten sample were recorded at primary incident electron energies of 1 keV, 2 keV and 3 keV by using the Ulvac-Phi model 5500 electron spectrometer, which is furnished with a concentric hemispherical analyzer. It maintains a constant overall energy resolution of ~ 0.33 eV, and the data were collected with an energy step of 0.05 eV in the constant analyzer energy mode. The angle of the incident electron beam was 0^0 and the detection angle of electron analyzer was 45^0 with respect to the surface normal. The measurements were carried out under analysis chamber pressures of less than 2.7×10^{-7} Pa.

Determination of energy loss function

The methodology of the RMC method has been comprehensively detailed in previous work [27–37]. Consequently, here only the most essential parts are presented. To extract ELF from REELS spectrum, a thorough analysis of electron-solid interactions is imperative while a Monte Carlo simulation of the REELS spectrum provides a natural and reasonable way for such an analysis.

Regarding electron elastic scattering, the ELSEPA code [39] was employed to calculate Mott's cross section [40]. The calculation of the elastic scattering cross section involves various alternative potential models including nuclear charge distribution, electron density, electron exchange potential, and correlation-polarization potential. Specifically, the Fermi distribution, numerical Dirac-Fock (DF) density, Furness-McCarthy exchange potential and the local-density approximation (LDA) are considered in the four aforementioned models, respectively.

In the case of electron inelastic scattering, a semi-classical model [41,42] based on the dielectric response theory was adopted. This model considers a depth-dependent DIIMFP, which offers a more accurate representation of the underlying physical phenomena, particularly the surface excitation effect. For an electron penetrating the surface from solid/vacuum side into the vacuum/solid side, the derived expression is as follows:

$$\begin{aligned}\sigma(z) = {} & \frac{2}{\pi v^2}\int_{q_-}^{q_+} \mathrm{d}q \frac{1}{q}\mathrm{Im}\left[\frac{-1}{\varepsilon(q,\omega)}\right]\Theta(-z) \\ & + \frac{4\cos\alpha}{\pi^3}\int_{q_-}^{q_+}\mathrm{d}q\int_0^{\frac{\pi}{2}}\mathrm{d}\theta\int_0^{2\pi}\mathrm{d}\phi\frac{q\sin^2\theta\cos(q_\perp z)\exp(q\|z)}{\widetilde{\omega}^2+q\|^2v_\perp^2} \\ & \times\left\{\mathrm{Im}\left[\frac{-1}{\varepsilon(q\|,\omega)+1}\right]-\frac{1}{2}\mathrm{Im}\left[\frac{-1}{\varepsilon(q\|,\omega)}\right]\right\}\Theta(-z)v_\perp > 0, \\ & + \frac{4\cos\alpha}{\pi^3}\int_{q_-}^{q_+}\mathrm{d}q\int_0^{\frac{\pi}{2}}\mathrm{d}\theta\int_0^{2\pi}\mathrm{d}\phi\frac{q\sin^2\theta\exp(-q\|z)}{\widetilde{\omega}^2+q\|^2v_\perp^2} \\ & \times\mathrm{Im}\left[\frac{-1}{\varepsilon(q\|,\omega)+1}\right]\left[2\cos\left(\frac{\widetilde{\omega}z}{v\cos\alpha}\right)-\exp(-q\|z)\right]\Theta(z)\end{aligned} \tag{1}$$

and

$$\begin{aligned}\sigma(z) = {} & \frac{2}{\pi v^2}\int_{q_-}^{q_+} \mathrm{d}q \frac{1}{q}\mathrm{Im}\left[\frac{-1}{\varepsilon(q,\omega)}\right]\Theta(-z) \\ & + \frac{4\cos\alpha}{\pi^3}\int_{q_-}^{q_+}\mathrm{d}q\int_0^{\frac{\pi}{2}}\mathrm{d}\theta\int_0^{2\pi}\mathrm{d}\phi\frac{q\sin^2\theta\cos(-q_\perp z)\exp(-q\|z)}{\widetilde{\omega}^2+q\|^2v_\perp^2} \\ & \times\mathrm{Im}\left[\frac{-1}{\varepsilon(q\|,\omega)+1}\right]\Theta(z)+\frac{4\cos\alpha}{\pi^3}\int_{q_-}^{q_+}\mathrm{d}q\int_0^{\frac{\pi}{2}}\mathrm{d}\theta\int_0^{2\pi}\mathrm{d}\phi v_\perp < 0, \\ & \times\frac{q\sin^2\theta\exp(q\|z)}{\widetilde{\omega}^2+q\|^2v_\perp^2}\left\{\mathrm{Im}\left[\frac{-1}{\varepsilon(q\|,\omega)+1}\right]-\frac{1}{2}\mathrm{Im}\left[\frac{-1}{\varepsilon(q\|,\omega)}\right]\right\} \\ & \times\left[2\cos\left(\frac{\widetilde{\omega}z}{v\cos\alpha}\right)-\exp(q\|z)\right]\Theta(-z)\end{aligned} \tag{2}$$

where $\widetilde{\omega} = \omega - qv\ \sin\theta\ \cos\phi\ \sin\alpha$, $q\| = q\sin\theta$, $v_\perp = v\cos\alpha$; the electron rest mass, electron charge and reduced Planck constant are set to 1 in the atomic unit ($m_e = e = \hbar = 1$). α is the angle between the incident electron and the surface normal, and $v = \sqrt{2E}$ is the velocity related to electron energy E. $\hbar\boldsymbol{q}$ and $\hbar\omega$ stand for momentum transfer and energy loss, respectively. The integration limits for q in Eqs. (1) and (2) are given by $q_\pm = \sqrt{2E} \pm \sqrt{2(E-\omega)}$. The bulk ELF, $\mathrm{Im}\{-1/\varepsilon(\boldsymbol{q},\omega)\}$ and surface ELF, $\mathrm{Im}\{-1/[\varepsilon(\boldsymbol{q}\|,\omega)+1]\}$ are included in the above DIIMFP equations. $\Theta(z)$ represents a step function about depth z.

The combination of Monte Carlo simulation of REELS spectrum and the MCMC updating of oscillator parameters constitutes a fundamental part of the RMC method. The purpose of this RMC method is to determine the optimal optical ELF, which minimizes the difference between

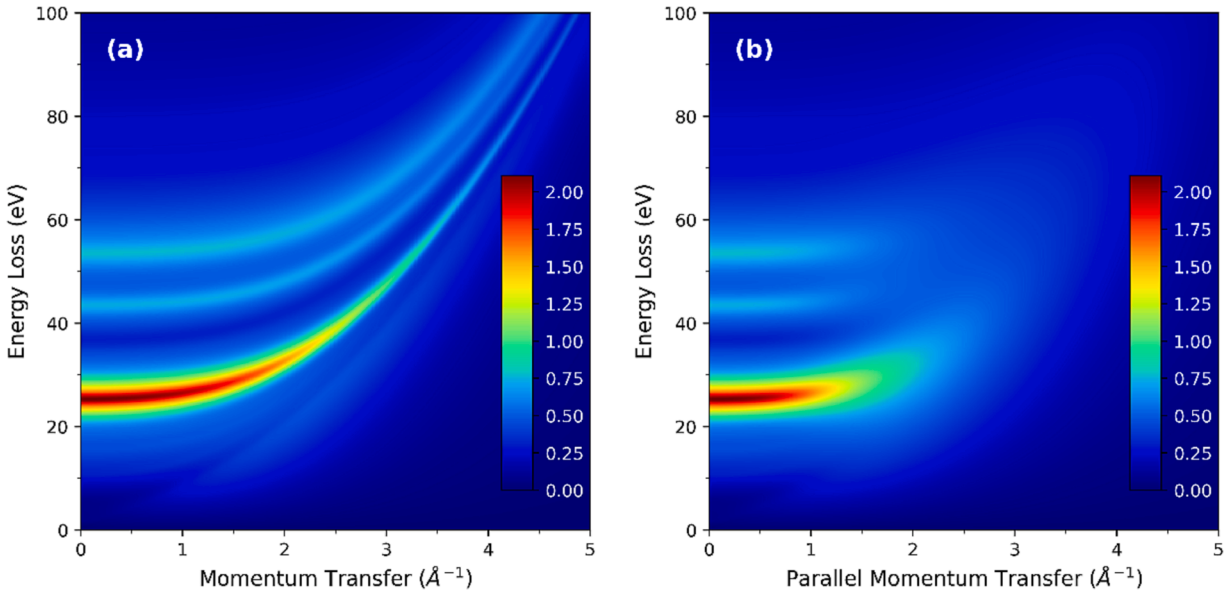

Fig. 1. 2D contour map of the extended (a) bulk and (b) surface ELFs by using Ritchie and Howie's dispersion relationship in the RMC procedure.

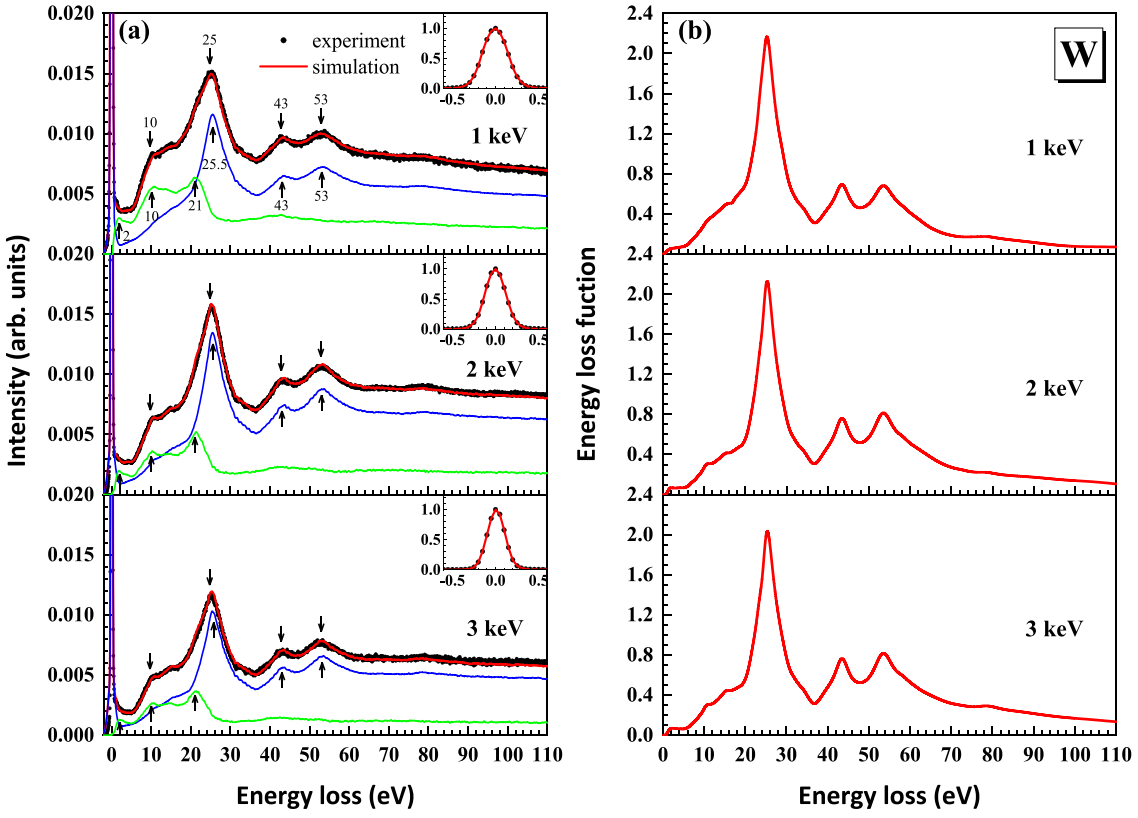

Fig. 2. (a) The simulated REELS spectra (red lines) and measured spectra (black lines) of tungsten at 1 keV, 2 keV and 3 keV. Contributions from surface and bulk excitations are separated from the simulated total spectrum and shown by the green and blue lines, respectively. The inset shows the elastic peak for convolution of the simulated spectrum. (b) The corresponding ELFs obtained from the simulated REELS spectra at each energy. (For interpretation of the references to colour in this figure legend, the reader is referred to the web version of this article.)

the simulated and the measured REELS spectra. A parameterized ELF is expressed as a summation of N Drude-Lindhard terms, characterized by 3 N oscillator parameters as inputs (the i th oscillator contains three parameters: oscillator strength A_i, energy ω_{pi}, and width γ_i) for the calculation of DIIMFP. Initially, these 3 N parameters are arbitrarily given. Through the comparison of the calculated REELS spectrum with experimental result the parameters are gradually updated by simulated annealing method [43] in a MCMC procedure until a satisfactory agreement was found between the simulated and the measured REELS spectra. The optimal optical ELF is thus obtained from the iterated ELF in a global optimization process. In the calculation, the parameterized optical ELF was extended into the momentum space through Ritchie and

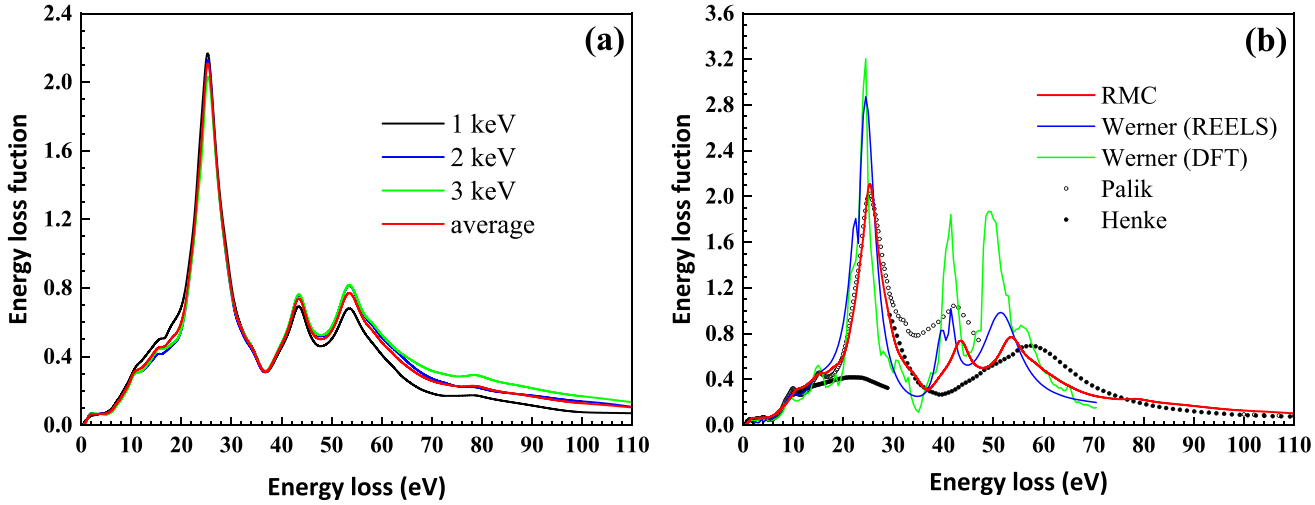

Fig. 3. (a) Comparison of the ELFs for three incident electron energies and the averaged ELF for tungsten. (b) Comparison of the averaged ELF obtained from the RMC method (red line) with Werner's REELS data (blue line) [22], Werner's DFT data (green line) [22], Palik's compiled data (open circles, lacking data in the energy loss range of 47–100 eV) [8], and Henke's data (solid circles) [10]. (For interpretation of the references to colour in this figure legend, the reader is referred to the web version of this article.)

Howie's method [44], and the plasmon dispersion relation $\omega_q^2(q,\omega_p) = \omega_p^2 + 2E_F q^2/3 + q^4/4$ is used, where E_F is the Fermi energy, ω_q is the extended energy loss and ω_p is the local plasmon energy loss. Fig. 1 shows the dispersions of bulk ELF and surface ELF from the final obtained oscillator parameters (i.e. averaged over three bulk ELFs) of tungsten.

Results and discussion

The ELF characterizes an intrinsic and bulk property of a material and is not dependent on the incident electron energy. To ensure the reliability of the determined ELF for the investigated material, conducting multiple measurements at different electron energies is essential. In this study the ELF data, covering an energy loss range of 0.1–110 eV, at electron incident energies of 1 keV, 2 keV and 3 keV are obtained.

In Fig. 2(a), we present the final simulated REELS spectra of tungsten alongside the corresponding measured spectra. The collection angle of signal electrons was taken as 5^0 in the simulation. A larger collection angle is useful to reduce the noise of the simulated spectrum and, hence, to accelerate the simulation and to derive more accurate ELF value. The elastic peak in an experimental spectrum (characterized by the loss energy ~ 0 with the peak width ~ 0.33 eV) in the simulated spectra was fitted to several Gaussian distributions and then used for convolution of simulated spectrum in the RMC procedure. Both the simulated and measured REELS spectra have been normalized with the intensity of their respective elastic peaks, as depicted in the inset of Fig. 2(a). It is clear that with the ELF finally obtained the simulation result agrees excellently with the experimental spectrum. Furthermore, we have differentiated the contributions arising from bulk and surface excitations in Fig. 2(a). For the calculation of the bulk contribution, the surface ELF terms in Eqs. (1) and (2) have been omitted from the DIIMFP, whereas the surface contribution is resulted from the exclusion of the bulk ELF term from the total spectrum. The ELFs for each investigated incident energy are shown in Fig. 2(b). As is shown in Fig. 2(a) that the overall shape of total spectrum closely mirrors that of bulk spectrum for higher energy losses exceeding 24 eV, which indicates that the bulk excitation mainly determines the shape above 24 eV while the surface excitation primarily influences the shape in the low energy loss range. At very low energy losses below 0.2 eV, the precision of the data is compromised due to the broadening of the elastic peak, leading to certain uncertainty in the obtained ELF results, which will be evaluated by the sum rules later. However, comparatively this energy broadening ~ 0.33 eV is quite smaller than that of many electron spectrometers.

Fig. 3(a) illustrates the comparison of ELFs obtained for three incident energies. These ELFs are quite similar in shape and slightly different in values. Quantitative agreement is found in the energy loss ranges of 0.1–10 eV and 21–42 eV. However, discernible differences in intensity is evident in the ranges of 10–21 eV and 42–110 eV, resulted from the experimental spectrum variation with the incident energy. Fig. 3(b) presents the averaged ELF over the three energies and the comparison with the literature data [8,10,22]. In contrast to Werner's data up to 70 eV by REELS measurement [22], the present ELF data by RMC analysis of REELS spectra cover a wider range of energy loss up to 110 eV. The present RMC result agrees well with Werner's data below 18 eV. And above 20 eV, both the present RMC and Werner's data reveal three significant characteristic peaks, exhibiting similar peak positions (around 25 eV, 43 eV, and 53 eV) but quite different intensities. In the energy loss range of 0.1–28 eV, our results are very close to that of Palik's data [8]. And in the range of 30–37 eV and for energy losses exceeding 78 eV, the present RMC data are closer to Henke's data [22].

Meanwhile, as is shown in Fig. 2(a), the bulk and the surface REELS spectra exhibit several obvious plasmon excitation peaks. Features located at ~ 2 eV, 10 eV and 21 eV on green lines were identified as surface plasmon excitations. Among these, the 2 eV and 21 eV peaks were observed in the research by Luscher [45], whereas the 10 eV peak was mentioned in the work of Edwards and Propst [46]. Furthermore, the simulated bulk REELS spectra also reveal peaks at ~ 25.5 eV, 43 eV and 53 eV on blue lines, which were recognized as bulk plasmon excitations. The 25.5 eV peak were the same as that in Luscher's work [45], while the 43 eV and 53 eV peaks were consistent with the results of Edwards and Propst's research [46]. In the overall REELS spectra, the peak at 10 eV can then be attributed to the 10 eV surface excitation contribution, whereas the peaks at 43 eV and 53 eV stem from the respective 43 eV and 53 eV bulk excitation contributions. The peak at 25 eV is actually composed of the 21 eV surface excitation and 25.5 eV bulk excitation. Therefore, in Fig. 3 all the surface features are well excluded from the bulk ELF and only three dominate bulk plasmon peaks at 25.5 eV, 43 eV and 53 eV are included.

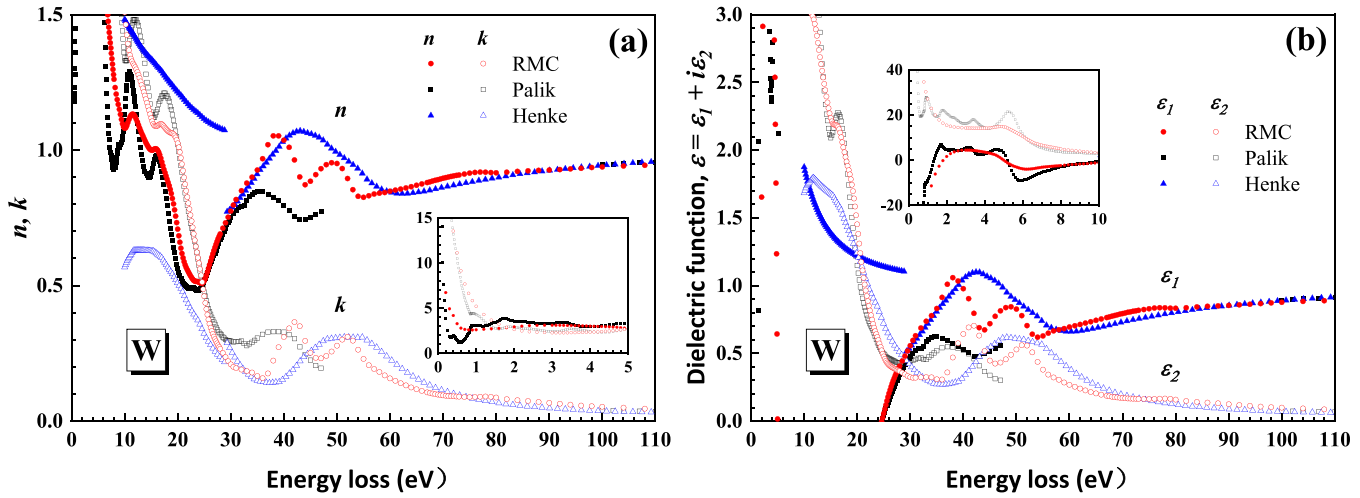

Fig. 4. (a) Plots of the refractive index n (red solid circles) and extinction coefficient k (red open circles) derived from the RMC method in comparison with Palik's data (black squares) and Henke's data (blue triangles). (b) Plots of the real part ε_1 (red solid circles) and imaginary part ε_2 (red open circles) derived from the RMC method in comparison with Palik's data (black squares) and Henke's data (blue triangles). (For interpretation of the references to colour in this figure legend, the reader is referred to the web version of this article.)

Table 1
List of the ps-sum and f-sum rules for tungsten at 1 keV, 2 keV, and 3 keV electron energies compared with those of Werner [22].

	$P_{\text{eff}}\|_{\text{ELF}}$ [a]	Relative error (%)	$Z_{\text{eff}}\|_{\text{ELF}}$ [b]	Relative error (%)	$Z_{\text{eff}}\|_{k}$ [b]	Relative error (%)	$Z_{\text{eff}}\|_{\varepsilon_2}$ [b]	Relative error (%)
1 keV	1.0169	1.69	72.2418	−2.38	70.9943	−4.06	71.3434	−3.59
2 keV	0.9957	−0.43	74.7759	1.05	74.3308	0.45	74.8117	1.10
3 keV	1.0083	0.83	76.4857	3.36	75.8120	2.45	76.1033	2.84
RMC (average)	1.0070	0.70	74.5011	0.68	73.7124	−0.39	74.0893	0.12
Werner (REELS)	1.039	3.9	71.5	−3.38	–	–	–	–
Werner (DFT)	1.012	1.2	72.7	1.76	–	–	–	–

[a] The theoretical nominal value for the *ps*-sum rule is unit.
[b] The theoretical nominal values for the *f*-sum rule of ELF, k, and ε_2 are the atomic number of tungsten, i.e. 74.

The dielectric function can then be derived from the optical ELF through the use of Kramers-Kronig relation, as [27]:

$$\varepsilon_1 = \frac{-\mathrm{Re}\{-1/\varepsilon(\omega)\}}{\mathrm{Im}\{-1/\varepsilon(\omega)\}^2 + \mathrm{Re}\{-1/\varepsilon(\omega)\}^2};$$
$$\varepsilon_2 = \frac{\mathrm{Im}\{-1/\varepsilon(\omega)\}}{\mathrm{Im}\{-1/\varepsilon(\omega)\}^2 + \mathrm{Re}\{-1/\varepsilon(\omega)\}^2}, \quad (3)$$

where ε_1 and ε_2 are the real and imaginary parts of dielectric function ε, respectively. Then the optical constants, i.e. the refractive index n and the extinction coefficient k, can be derived as [27]:

$$n = \sqrt{\frac{\varepsilon_1 + \sqrt{\varepsilon_1^2 + \varepsilon_2^2}}{2}};$$
$$k = \sqrt{\frac{-\varepsilon_1 + \sqrt{\varepsilon_1^2 + \varepsilon_2^2}}{2}}. \quad (4)$$

Applying Eqs. (3) and (4), we have successfully obtained the optical constants and dielectric function of tungsten from the averaged optical

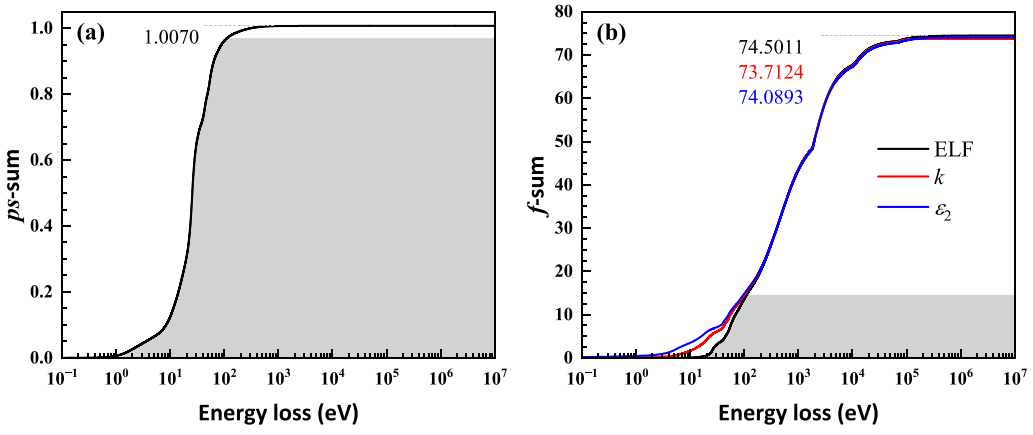

Fig. 5. (a) Calculation for *ps*-sum rule of ELF. (b) Calculation for *f*-sum rule of ELF, k and ε_2.

ELF derived by the RMC method, as illustrated in Fig. 4. Comparison between the RMC derived optical constants and the data in Palik's database up to energy loss of 28 eV demonstrates similar trends and characteristics. And congruence with Henke's data is evident for energy losses exceeding 78 eV. The distinctions are found in the intermediate energy loss range between 28 eV and 78 eV. These aforementioned conclusions closely paralleled the findings drawn from the ELF comparisons highlighted in Fig. 3(b).

The accuracy of the present ELFs determined through the RMC method were verified by the *ps*- and *f*-sum rules [38]. As is shown in Fig. 3(a), the ELFs at the three incident energies are not completely coincide with each other at the higher energy losses. The sum rules were calculated for the present ELFs, the extinction coefficient k and the imaginary part ε_2 of dielectric function below 110 eV in combination with the data from Henke [10] (from 140 eV to 30 keV), EPDL97 [47] (from 30 keV to 10 MeV) and interpolation of ELFs and Henke's data in the range of 110–140 eV in order to ensure the continuity of data for sum rules. Table 1 lists the convergence values of both the *ps*- and *f*-sum rules for the ELFs at three incident electron energies along with the averaged ELF, and the comparison with the sum rule results in Werner's work [22]. The theoretical nominal values are unit and atomic number for the *ps*- and *f*-sum rules, respectively. It can be seen from Table 1 that the present RMC averaged ELF is very accurate and the relative errors for the *ps*- and *f*-sum rules are merely 0.70 % and 0.68 %, respectively. The contributions to the *ps*- and *f*-sum rules from the averaged ELF, extinction coefficient k, or the imaginary part ε_2 of dielectric function at 0.1–110 eV obtained by the RMC method are visually shown by the shadow areas in Fig. 5. The shadow areas correspond to approximately 96.21 % and 19.48 % for the contribution from the present data to the total calculation of the *ps*- and *f*-sum rules, respectively. In Fig. 5(a), the *ps*-sum rule approaches a convergence value of 1.0070, which is very close to the theoretical value. In Fig. 5(b), the results for the *f*-sum rules of ELF, k, and ε_2 are 74.5011, 73.7124 and 74.0893, respectively. The associated relative errors are limited to 0.68 %, −0.39 % and 0.12 %, respectively.

Conclusions

By employing the RMC method, we have successfully simulated the REELS spectra of tungsten at the incident electron energies of 1 keV, 2 keV and 3 keV. The separation of surface and bulk REELS spectra was effectively achieved through the utilization of surface and bulk DIIMFP in our simulation procedure. This allows a highly accurate ELF of tungsten to be derived via our RMC analysis procedure, which is important in calculating optical constants and the dielectric function. The present ELF exhibited minuscule relative errors of 0.70 % and 0.68 % for the *ps*- and *f*-sum rules, respectively. The high accuracy of the derived ELF and optical constants will be beneficial for their practical applications.

CRediT authorship contribution statement

Z. Li: Writing – original draft, Investigation, Formal analysis. **J.M. Gong:** Investigation. **Y. Harada:** Investigation. **B. Da:** Software, Methodology, Conceptualization. **R.G. Zeng:** Software, Funding acquisition. **Z.J. Ding:** Conceptualization, Software, Methodology, Writing – review & editing, Supervision, Project administration.

Declaration of competing interest

The authors declare that they have no known competing financial interests or personal relationships that could have appeared to influence the work reported in this paper.

Data availability

Data will be made available on request.

Acknowledgements

This work was supported by the Fund of Science and Technology on Surface Physics and Chemistry Laboratory (XKFZ202103), Chinese Education Ministry through "111 Project 2.0" (BP0719016), the National Institute for Materials Science under the support system for curiosity-driven research, JSPS KAKENHI Grant Number JP21K14656, the The Kurata Grants from The Hitachi Global Foundation and from The Iketani Science & Technology Foundation. We thank Prof. H.M. Li and the supercomputing center of USTC for the support of parallel computing.

References

[1] Wischnitzer S. Introduction to Electron Microscopy. Pergamon Press; 1970.
[2] Cricenti A, Paparazzo E, Scarselli MA, Moretto L, Selci S. Preparation and characterization of tungsten tips for scanning tunneling microscopy. Rev Sci Instrum 1994;65:1558–60.
[3] Koperski M, Nogajewski K, Arora A, Cherkez V, Mallet P, Veuillen J-Y, et al. Single photo emitters in exfoliated WSe_2 structures. Nat Nanotechnol 2015;10:503–6.
[4] Zhang YJ, Oka T, Suzuki R, Ye JT, Iwasa Y. Electrically switchable chiral light-emitting transistor. Science 2014;344:725–8.
[5] Zhou HL, Wang C, Shaw JC, Cheng R, Chen Y, Huang XQ, et al. Large area growth and electrical properties of p-type WSe_2 atomic layers. Nano Lett 2015;15:709–13.
[6] Huang ZF, Song JJ, Pan L, Zhang XW, Wang L, Zou JJ. Tungsten oxides for photocatalysis, electrochemistry, and phototherapy. Adv Mater 2015;27:5309–27.
[7] Thummavichai K, Xia YD, Zhu YQ. Recent progress in chromogenic research of tungsten oxides towards energy-related applications. Prog Mater Sci 2017;88:281–324.
[8] Palik ED, editor. Handbook of Optical Constants of Solids. Academic Press; 1985.
[9] Weaver JH, Olson CG, Lynch DW. Optical properties of crystalline tungsten. Phys Rev B 1975;12:1293–7.
[10] Henke BL, Lee P, Tanaka TJ, Shimabukuro RL, Fujikawa BK. Low-energy X-ray interaction coefficients: photoabsorption, scattering, and reflection E=100-2000 eV, Z=1-94. At Data Nucl Data Tables 1982;27:1–144.
[11] Egerton RF. Electron Energy Loss Spectroscopy in the Electron Microscope. 2nd ed. New York: Plenum Press; 1986.
[12] Daniels J, Festenberg CV, Raether H, Zeppenfeld K. Optical Constants of Solids by Electron Spectroscopy. New York: Springer; 1970.
[13] Ohno Y. Kramers-Kronig analysis of reflection electron-energy-loss spectra measured with a cylindrical mirror analyzer. Phys Rev B 1989;39:8209.
[14] Yubero F, Tougaard S. Model for quantitative analysis of reflection-electron-energy-loss spectra. Phys Rev B 1992;46:2486.
[15] Yubero F, Tougaard S, Elizalde E, Sanz JM. Dielectric loss function of Si and SiO_2 from quantitative analysis of REELS spectra. Surf Interface Anal 1993;20:719–26.
[16] Ding ZJ, Shimizu R. Monte Carlo simulation study of reflection-electron-energy-loss-spectroscopy spectrum. Phys Rev B 2000;61:14128.
[17] Ding ZJ, Li HM, Pu QR, Zhang ZM, Shimizu R. Reflection electron energy loss spectrum of surface plasmon excitation of Ag: A Monte Carlo study. Phys Rev B 2002;66:085411.
[18] Ding ZJ. Inelastic scattering of electrons at real metal surfaces. Phys Rev B 1997;55:9999.
[19] Ding ZJ. Self-energy in surface electron spectroscopy: I. Plasmons on a free-electron-material surface. J Phys: Condens Matter 1998;10:1733–51.
[20] Ding ZJ. Self-energy in surface electron spectroscopy: II. Surface excitation on real metal surfaces. J Phys: Condens Matter 1998;10:1753–65.
[21] Werner WSM. Differential surface and volume excitation probability of medium-energy electrons in solids. Phys Rev B 2006;74:075421.
[22] Werner WSM, Glantschnig K, Ambrosch-Draxl C. Optical constants and inelastic electron-scattering data for 17 elemental metals. J Phys Chem Ref Data 2009;38:1013–92.
[23] Da B, Mao SF, Sun Y, Ding ZJ. A new analytical method in surface electron spectroscopy: reverse Monte Carlo method, e-J. Surf Sci Nanotechnol 2012;10:441–6.
[24] Da B, Sun Y, Mao SF, Zhang ZM, Jin H, Yoshikawa H, et al. A reverse Monte Carlo method for deriving optical constants of solids from reflection electron energy-loss spectroscopy spectra. J Appl Phys 2013;113:214303.
[25] Sun Y, Xu H, Da B, Mao SF, Ding ZJ. Calculations of energy-loss function for 26 materials. Chin J Chem Phys 2016;29:663.
[26] Yang LH, Da B, Tőkési K, Ding ZJ. Individual separation of surface, bulk and begrenzungs effect components in the surface electron energy spectra. Sci Rep 2021;11:5954.
[27] Xu H, Da B, Tóth J, Tőkési K, Ding ZJ. Absolute determination of optical constants by reflection electron energy loss spectroscopy. Phys Rev B 2017;95:195417.
[28] Xu H, Yang LH, Da B, Tóth J, Tőkési K, Ding ZJ. Study of optical and electronic properties of nickel from reflection electron energy loss spectra. Nucl Instr Meth B 2017;406:475–81.

[29] Xu H, Yang LH, Tóth J, Tőkési K, Da B, Ding ZJ. Absolute determination of optical constants of three transition metals using reflection electron energy loss spectroscopy. J Appl Phys 2018;123:043306.
[30] Yang LH, Menyhárd M, Sulyok A, Tőkési K, Ding ZJ. Optical properties and excitation energies of iridium derived from reflection electron energy loss spectroscopy spectra. Appl Surf Sci 2018;456:999–1003.
[31] Yang LH, Tőkési K, Da B, Ding ZJ. Determination of electron inelastic mean free path of three transition metals from reflection electron energy loss spectroscopy spectrum measurement data. Eur Phys J D 2019;73:1–19.
[32] Yang LH, Tőkési K, Tóth J, Da B, Li HM, Ding ZJ. Optical properties of silicon and germanium determined by high-precision analysis of reflection electron energy loss spectroscopy spectra. Phys Rev B 2019;100:245209.
[33] Yang LH, Tőkési K, Tóth J, Da B, Ding ZJ. Revision of optical property of silicon by a reverse Monte Carlo analysis of reflection electron energy loss spectroscopy spectra. J Phys: Conf Ser 2020;1412:202026.
[34] Yang LH, Gong JM, Sulyok A, Menyhárd M, Sáfrán G, Tőkési K, et al. Optical properties of amorphous carbon determined by reflection electron energy loss spectroscopy spectra. Phys Chem Chem Phys 2021;23:25335–46.
[35] Gong JM, Tőkési K, Liu X, Da B, Yoshikawa H, Tanuma S, et al. Determination of electron inelastic mean free path and stopping power of hafnium dioxide. Results Phys 2023;51:106609.
[36] Yang TF, Zeng RG, Yang LH, Sulyok A, Menyhárd M, Tőkési K, et al. Energy loss function of samarium. Sci Rep 2023;13:3909.
[37] Li Z, Gong JM, Da B, Tóth J, Tőkési K, Zeng RG, et al. Improved reverse Monte Carlo analysis of optical property of Fe and Ni from reflection electron energy loss spectroscopy spectra. Sci Rep 2023;13:12480.
[38] Tanuma S, Powell CJ, Penn DR. Use of sum rules on the energy-loss function for the evaluation of experimental optical data. J Electron Spectros Relat Phenomena 1993;62:95–109.
[39] Salvat F, Jablonski A, Powell CJ. ELSEPA Dirac partial-wave calculation of elastic scattering of electrons and positrons by atoms, positive ions and molecules. Comput Phys Commun 2005;165:157–90.
[40] Mott NF. The scattering of fast electrons by atomic nuclei. Proc r Soc London A 1929;124:425–42.
[41] Li YC, Tu YH, Kwei CM, Tung CJ. Influence of the direction of motion on the inelastic interaction between electrons and solid surfaces. Surf Sci 2005;589:67–76.
[42] Da B, Mao SF, Ding ZJ. Validity of the semi-classical approach for calculation of the surface excitation parameter. J Phys: Conden Matter 2011,;23:395003.
[43] Kirkpatrick S, Gelatt CD, Vecchi MP. Optimization by simulated annealing. Science 1983;220:671–80.
[44] Ritchie RH, Howie A. Electron excitation and the optical potential in electron microscopy. Philos Mag 1977;36:463–81.
[45] Luscher PE. Energy loss mechanisms in low energy electron scattering from W(100) and their use as a surface sensitive spectroscopy. Surf Sci 1977;66:167–88.
[46] Edwards D, Propst FM. Energy loss spectra of inelastically scattered electrons from tungsten. J Chem Phys 1971;55:5175–8.
[47] Cullen DE, Hubbell JH, Kissel L. EPDL97: The Evaluated Data Library, 1997 Version. Livermore, CA: Lawrence Livermore National Lab; 1997.